Fabrication and Characterization of Quaternary Catalyst Co-Fe-Mn-Ni for Enhancing both Hydrogen and Oxygen Evolution Reactions

Ibrahim S. El-Hallag[1], * Ahmad A. Al-Owais[2] and Safya Elsharkawy[1]

[1]*Lab of Electrodeposition and Nanomaterials, Chemistry Department, Faculty of Science, Tanta University, Egypt*

[2]*Chemistry Department, College of Science, King Saud University, Saudi Arabia*

*Corresponding author: i.elhallag@yahoo.com

Received 05/05/2025; accepted 02/10/2025
https://doi.org/10.4152/pea.2027450503

Abstract

The transition towards sustainable energy sources requires the development of cost-effective and highly efficient electrocatalysts for water electrolysis. This study reports the fabrication and optimization of a non-precious bifunctional quaternary electrocatalyst from Co-Fe-Mn-Ni (CFMN) via electrodeposition for water-splitting reactions of both hydrogen (HER) and oxygen evolution (OER) reactions. Physicochemical characterizations showed that optimized quaternary CFMN electrocatalyst, deposited from an acetate electrolyte, had a composition of $Co_{1.54}$-$Fe_{0.11}$-$Mn_{0.01}$-$Ni_{0.043}$, with polycrystalline nanosheet morphology. Electrochemical activity assessment revealed remarkable electrocatalytic performance for both HER and OER, surpassing that of single-metal catalysts. CFMN electrocatalyst displayed an overpotential (η) of −110 and 310 mV, with current density values of 8.3 x 10^{-4} and 4.5 x 10^{-2} A/cm^{-2}, for HER and OER, respectively. Moreover, the catalyst exhibited excellent stability, retaining over 86.3% of its initial current density during 4000 s of chronoamperometric testing and showing negligible performance degradation after 1000 continuous linear sweep voltammetry cycles. This study aims to contribute to the advancement of multi-element, efficient and cost-effective electrocatalysts for water-splitting reactions and hydrogen fuel production.

Keywords: Acetate bath; bifunctional catalysts; Co-Ni-Mn-Fe electrocatalyst; fabrication; Hydrogen evolution reaction; Oxygen evolution reaction; renewable energy.

Introduction•

It has been challenging to use aqueous electrolytes to electrodeposit transition metals, due to high overpotential, which leads to a rapid competing hydrogen

• The abbreviations and symbols definition lists are in pages 378-79.

evolution reaction (HER) at the cathode [1]. This often results in thin, brittle, and uneven deposits with low current efficiencies. Despite this, there have been successful observations of metallic Mo being deposited using concentrated acetate-based aqueous electrolytes. This allows for the creation of Mo coatings at temperatures close to room temperature and neutral pH, without the need for expensive conditions or reagents [1]. Furthermore, [2] has noted successful formation of Zn-Ni binary alloys on steel substrates using an acetate-based bath. By controlling pH within a specific range, the authors have suggested that each metal was independently deposited through two successive one-electron transfer steps. However, contrary to expectations, co-deposits rich in Zn were consistently obtained. It was found that, at low current densities (< 0.7 A/cm^2), the coating had a porous layer of nodular, randomly orientated grains. With higher current densities, the formation of more uniform coatings with smaller, smoother and more compact grains was observed. Additionally, using an acetate bath offers the advantage of producing high-quality, bright deposits with improved cathode efficiency and more cost-effective waste treatment.

Hydrogen is regarded as the most promising renewable and sustainable energy source, due to its abundant, high energy density (140 MJ kg^{-1}) and long-term sustainability as ultimate zero-emission energy source [3-9]. However, only about 7% of global hydrogen production is obtained by sustainable water electrolysis, which theoretically presents a simplistic, economical and effective approach for production of pure oxygen and hydrogen without generating any pollutants [10-13]. However, in water electrochemical splitting in alkaline media, kinetics of both oxygen evolution reaction (OER) and hydrogen evolution reaction (HER) are slow and require high overpotential to proceed [14-16]. Thus, it is imperative to develop an intrinsic electrocatalyst with high electrocatalytic activity. Currently, although most suitable electrocatalysts for HER and OER are noble metal-based materials such as Pt, Ru or Ir, respectively, they are restricted in large-scale applications, due to their high cost and limited availability [17-20]. To address these challenges, it is imperative to develop bifunctional noble metal-free electrocatalysts that have unique properties and high activity towards both HER and OER in alkaline electrolytes [21-24]. Therefore, various bifunctional catalysts based on transition metals show promise for water splitting, including metal carbides [25, 26], nitrides [27, 28] phosphates [29-33] and sulphides [34, 35], owing to their unique surface structures and functionality. Thus, numerous strategies have been employed to design electrocatalysts and develop their surface electronic structure and functionality with more active sites to enhance their catalytic performance. For example, Ni-Fe alloys have been considered promising candidates for water splitting, due to their impressive catalytic activity, affordability and high abundance [36]. Incorporating

Fe into a binary Ni-Co alloy spine-type oxide and modifying its electronic structure to achieve excellent HER catalytic activity has been proposed by [37]. In a related study, a mesoporous ternary CoFeNi oxide (CoFeNi-O) electrocatalyst prepared via a dealloying process revealed enhanced water electrocatalytic splitting activity and very low overpotentials of 200 and 57.9 mV for OER and HER, respectively. Additionally, a cell overpotential gap of 1.56 V was enough to drive water-splitting reactions at 10 mA/cm^2 [38]. Moreover, [39] has prepared a Ni-Fe-P electrode with intrinsic catalytic activity towards HER in 0.5 M H_2SO_4. Trimetallic NiFeMo electrocatalysts have shown a 1.45 V overall water splitting potential at 10 mA/cm^2, as a result of low overpotentials and Tafel slopes for HER and OER [40]. This electrocatalytic activity enhancement was attributed to the incorporation of high-valence metals (e. g. V, Cr and/or Mn) into Fe-Co-Ni electrocatalysts, which induced surface reconstruction, defects and vacancies that significantly improved water-splitting reactions [41, 42]. Particularly, the use of Mn, among other abundant earth metals, can tailor the electronic structure and improve catalytic activity. In this regard, [43] has proposed that Ni-Fe-Mn has impressive catalytic performance and durability towards OER. Very recent work has shown that a quaternary alloy system such as Cu–Ni–Co–Fe exhibits excellent high hydrogen storage and high stability with minimal structure degradation [44]. This system also displays superiority during long-term water electrolysis. Also, it was established that NiFeCrCo LDH (Layered Double Hydroxide) alloy enhances the performance of OER and HER, which provides a new perspective on utilizing entropy effects in LDH as high-performance overall water electrolysis catalysts [45]. The importance of abundant earth metals and the need for improving an electrode consisting of low-priced and abundant metals inspired the authors of the present study to propose a quaternary alloy consisting of four abundant and available metals, such as Co, Fe, Mn and Ni (CFMN), for overall water splitting reactions [46]. The advantages of ternary and quaternary electrocatalysts are that they not only preserve intrinsic properties of component elements but also generate new interfaces and create defects, active sites and vacancies due to lattice distortion. Consequently, it modifies the electronic structure, accelerates electron and proton transfer, and moderates reactants' and intermediates adsorption energy at the catalyst surface [42-47]. Herein, two goals have been set: to use a one-step electrodeposition strategy to prepare an electrode of a single metal component and demonstrate its catalytic behaviour towards HER and OER; and to synthesize a quaternary electrocatalyst of Co, Fe, Mn and Ni (CFMN), studying its catalytic activity towards HER and OER. Additionally, a comparative evaluation of the electrochemical activity of the single quaternary (CFMN) electrocatalysts towards HER and OER was conducted, analysing their morphology, compositions, structures and kinetics.

Materials and methods

Reagents and preparations

High-purity chemicals (99%), including nickel chloride hexahydrate ($NiCl_2.6H_2O$), cobalt chloride hexahydrate ($CoCl_2.6H_2O$), ferric chloride ($FeCl_3$), manganese chloride ($MnCl_2.4H_2O$), sodium acetate trihydrate ($CH_3COONa.3H_2O$), acetic acid (CH_3COOH) and potassium hydroxide (KOH) were obtained from Sigma-Aldrich. These chemicals were used without further purification. Milli-Q ultrapure water purification system was used to obtain deionized water that was used to prepare solutions in all experiments.

Electrodeposition of Co, Fe, Mn, Ni and CoFeMnNi (CFMN) electrocatalysts

Electrodeposition of Co, Fe, Mn, Ni and quaternary CFMN electrocatalysts was performed using a 25 mL glass cell with a three-electrode configuration. Electrodeposition of individual metals (Co, Fe, Mn, and Ni) on a graphite electrode (3 mm diameter) was achieved from the metal salt dissolved in an acetate buffer solution at pH 4.6. An acetate buffer solution comprising 0.2 M sodium acetate and 0.2 M acetic acid was typically prepared and adjusted to the desired pH of 4.6 using 0.1 M NaOH, while metal salts were dissolved in the electrolyte at a concentration of 0.4 M for electrodeposition of each metal. The solution used to fabricate quaternary CFMN electrocatalyst was prepared by mixing 0.25 M $CoCl_2.6H_2O$, 0.05 M $FeCl_3$, 0.1 M $MnCl_2.4H_2O$ and 0.15 M $NiCl_2.6H_2O$ (corresponding to a molar ratio of 5:1:2:3) in a 0.4 M acetate buffer solution at a pH of 4.6. Cyclic voltammetry was first performed to determine the appropriate deposition potential at −1.15, −1.25, −1.43, −1.1 and −1.15 V *vs.* Ag/AgCl for Co, Fe, Mn, Ni and quaternary CFMN electrocatalysts, respectively.

Physicochemical and electrochemical characterizations

Scanning electron microscopy (SEM) and energy dispersive X-ray (EDX) analyses were performed for electrocatalysts using SEM JEOL, JSM IT-100, with a maximum magnification of 300,000 x, maximum resolution of 3 nm and a maximum acceleration voltage of 30 kV. Transmission electron microscopy (TEM) was performed using TEM JEOL, JEM-200, with a maximum magnification of 1.5 million x. X-ray diffraction (XRD) patterns were recorded using Shimadzu XRD 6000, x-ray diffractometer Cu $K_{\alpha 1}$ (wavelength = 1.5418 A^0). Electrodeposition process and electrochemical characterizations were performed using a computer-controlled potentiostat/galvanostat model 273 A, from Princeton Applied Research, Oak Ridge, TN, USA, with 270/250-PAR software. Before each deposition process, the graphite working electrode (diameter 2.0 mm) was cleaned with concentrated hydrochloric acid to remove any oxides or impurities attached to the surface, cleaned with polishing paper grade 100, and then rinsed thoroughly with distilled

water. Electrochemical performance of electrodeposited electrodes was studied in a standard three-electrode system, with fabricated electrocatalysts used as working electrodes, and Ag/AgCl (3 M KCl) and Pt wire used as reference and counter electrodes, respectively. Linear sweep voltammetry (LSV) measurements were performed to study HER and OER in a 1.0 M KOH solution. All potential data or overpotentials for the fabricated electrodes were referred to as reversible hydrogen electrode (RHE).

Results and discussion

Characterisation of the Co, Ni, Mn, Fe and quaternary CFMN electrocatalysts

Surface morphology of Co, Ni, Mn, Fe and quaternary CFMN electrocatalysts was examined using SEM, and images are presented in Fig. 1 (a-e. Deposited Co film showed a uniform distribution in the form of rosette-flower-like nanoparticles, as shown in Fig. 1a.

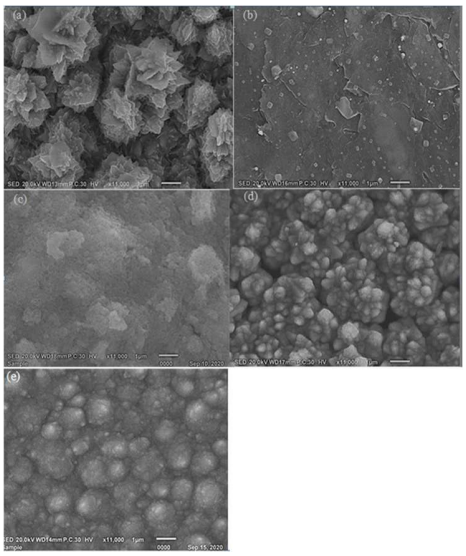

Figure 1: SEM images of a) Co, b) Fe, c) Mn, d) Ni, and e) CoFeMnNi deposits.

SEM image of Fe electrocatalyst in Fig. 1b showed a random distribution with cubic-shaped crystals that failed to cover the whole graphite surface, indicating difficulty in electrodeposition. Deposited Mn film provided surface coverage and formed small fibrous aggregates (Fig. 1c), while Ni deposit appeared in a cauliflower structure with uniform distribution (Fig. 1d). In contrast, SEM image of deposited quaternary CFMN electrocatalyst displays a uniformly distributed, compact and dense surface with a bubble shape, as shown in Fig. 1e. It was established that several mechanisms have been proposed to illustrate anomalous co-deposition phenomenon, including Matlosz model, which shows that reduction of

Fe^{2+} and Ni^{2+} takes place via two steps, and that from Fe^{3+} via three steps, as shown in Eqs. (1) and (2), respectively [48-50]. Reduction of Ni or Fe ions occurs through multiple steps, as shown in Eqs. (1-5), and reduction rate of Fe^{+}_{ads} is higher than that of Ni^{+}_{ads}. This results in a higher proportion of Fe^{+}_{ads} coverage on the surface, which inhibits further reduction of Ni^{+}_{ads} ions [51-52].
In the case of Fe^{2+} or Ni^{2+} ions:

$$M^{+2} + e^{-} \rightarrow M^{+}_{ads} \quad (1)$$

$$M^{+}_{ads} + e^{-} \rightarrow M \quad (2)$$

In the case of Fe^{3+} ions:

$$Fe^{+3} + e^{-} \rightarrow Fe^{+2}_{ads} \quad (3)$$

$$Fe^{+2}_{ads} + e^{-} \rightarrow Fe^{+}_{ads} \quad (4)$$

$$Fe^{+}_{ads} + e^{-} \rightarrow Fe \quad (5)$$

Moreover, the internal structure of the quaternary CFMN electrocatalyst was further investigated using TEM analysis. Fig. 2 presents TEM images of a thick (a) and thin (b) layer of deposited CFMN film that had been scratched from graphite substrate.

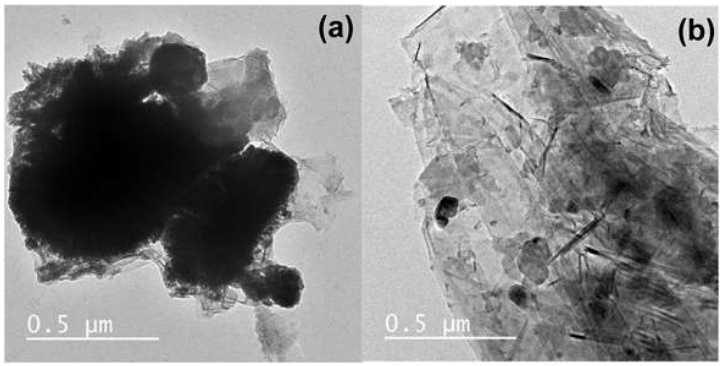

Figure 2: TEM images of deposited quaternary CFMN electrocatalyst- **(a)** with thick and uneven edges and **(b)** with a thin polycrystalline film.

TEM image in Fig. 2a shows formation of thick deposits with unevenly thin edges, while in Fig. 2b it provides conclusive evidence of formation of very thin nanosheets of polycrystalline CFMN electrocatalysts. Moreover, TEM analysis also revealed presence of small crystallites with sizes ranging from a few to tens of nanometers attributed to the various alloying elements. Formation of these small crystallites suggests that the fabrication process involved heterogeneous nucleation and growth mechanisms, consistent with previous studies on nanocrystalline alloys [48, 49]. Fig. 3 shows XRD patterns of Co, Fe, Mn, Ni and quaternary CFMN electrocatalysts.

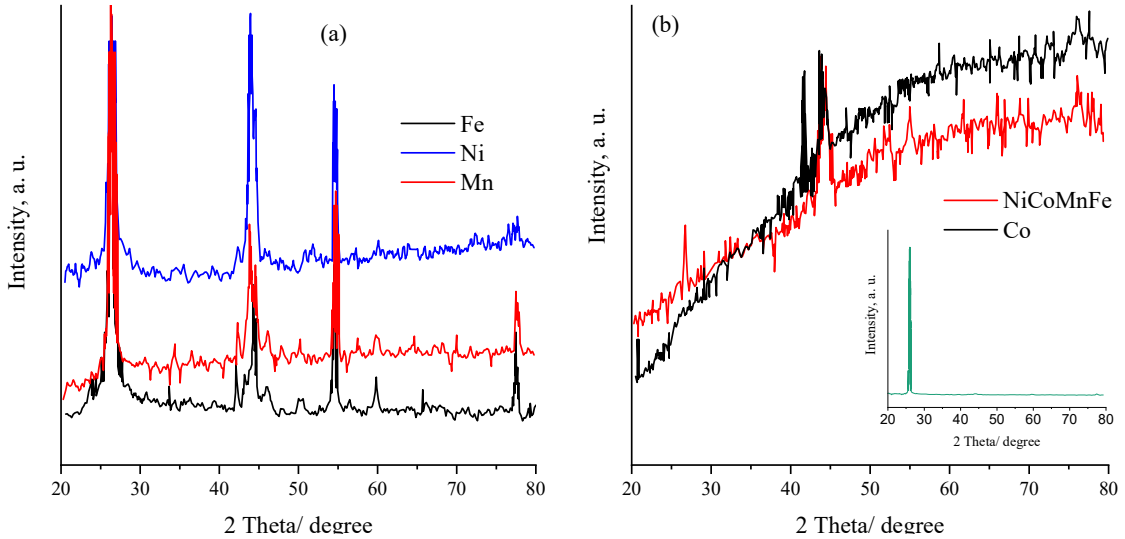

Figure 3: (a) XRD spectra of deposited Fe, Mn and Ni films; **(b)** XRD spectra of deposited Co and CNMF alloys; inset graph relates to XRD spectrum of bare PGE substrate.

XRD of Fe, Mn and Ni deposits (Fig. 3a) shows a high-intensity peak at 2θ value = 26°, due to graphite substrate. Deposited Fe nanoparticles showed three main diffraction peaks (Fig. 4a) for body-centered cubic phase (BCC) at 2θ values of 44.3°, 62.2°. and 78.4°, corresponding to diffraction planes (110), (200) and (211), respectively (JCPDS card No. 01-085-1410). Average crystallite size of deposited Fe nanoparticles, calculated from Scherrer equation, was 39 ± 2 nm. Deposited Ni (Fig. 3a) showed three diffraction peaks at 2θ values of 43.8°, 44.4° and 52.2°, corresponding to diffraction planes (111), (111) and (200), respectively (JCPDS card No. 041-0850). Deposited Mn nanoparticles showed main diffraction peak at 2θ = 43.8° and smaller intensity diffraction peaks at 2θ values of 44.7°, 54.8° and 77.8°, matching diffraction planes of (310), (321) and (510), respectively (JCPDS card No.00-003-1014). Average size of Mn was 26.5 ± 2 nm. Moreover, XRD of deposited Co nanoparticles in Fig. 3b showed two main diffraction peaks with high intensity at 2θ values of 41.4° and 44.2°, corresponding to diffraction planes (100) of hexagonal closed-packed (HCP) and face-centred cubic (FCC) phases, respectively (JCPDS card No. 01-089-4308). Average crystallite size of deposited Co nanoparticles was 24.8 ± 2 nm. In the case of deposited quaternary CFMN electrocatalyst, XRD pattern in Fig. 3b revealed three peaks, the first at 2θ = 44.2°, with high intensity attributed to (111) diffraction plane of FCC phase. The other two peaks at 2θ = 52.2° and 76° correspond to (200) and (220) diffraction planes, respectively, related to orientations of pure FCC Ni and Co (JCPDS No. 70-1849). Absence of diffraction peaks for Mn and Fe suggests formation of a solid solution due to substitution of Ni or Co atoms by Mn and Fe atoms, leading to a highly enriched Ni cubic FCC structure with substituted atoms. Average crystallite size of deposited quaternary CFMN electrocatalyst was 21.2 ± 2 nm.

Electrocatalytic water splitting

Comparative electrocatalytic HER activity

Electrodeposition process of Co, Fe, Mn, Ni and quaternary CFMN electrocatalysts was optimized based on their electrocatalytic efficiency towards HER. Fig. 4(a) shows polarization curves of LSV for HER in 1.0 M KOH, at a scan rate of 5.0 mV/s, at 298K, using Co, Fe, Mn, Ni and quaternary CFMN electrocatalysts deposited from an acetate bath. As shown in Table 1, deposited metals of Fe, Ni, Co and Mn electrodes exhibited an overpotential (η) of −264 ± 4, −194 ± 4, −164 ± ,4, and −134 ± 4 mV for HER, to produce a current density of 10 mA/cm^2, respectively. In contrast, deposited quaternary CFMN electrocatalysts exhibited least negative overpotential value of −110 ± 4 mV, indicating their higher catalytic activity for HER.

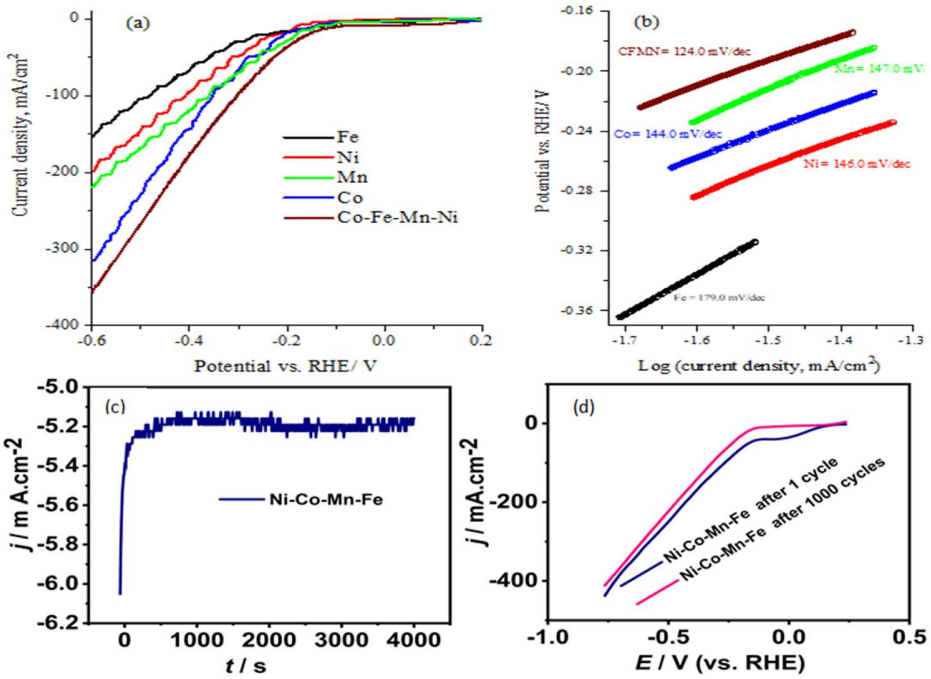

Figure 4: (a) LSV at 5.0 mV/s recorded during HER in 1.0 M KOH with Co, Fe, Mn and Ni and quaternary CFMN electrocatalyst deposited from acetate buffer at -1.15 V for 4000 s; **(b)** Tafel plots; **(c)** chronoamperometry curve of CFMN at –0.10 V *vs.* RHE and 298° K; and **(d)** polarization curves at CFMN in 1.0 M KOH after the first and 1000 cycles.

Fig. 4(b) presents corresponding HER Tafel plots of polarization curves from Co, Fe, Mn, Ni and quaternary CFMN electrocatalysts. Tafel slope is a parameter that provides information about rate-limiting step of electrocatalytic reaction. Quaternary CFMN electrocatalyst exhibited a Tafel slope of 124 ± 4 mV/dec, indicating a faster reaction rate compared to the one from deposited Fe nanoparticles, which exhibited a Tafel slope of 179 ± 4 mV dec^{-1}.

Observed differences in Tafel slopes from deposited metals and quaternary CFMN electrocatalysts highlight the importance of composition and morphology of electrocatalysts in determining its electrocatalytic activity towards HER. Reaction mechanism of HER in the alkaline solution and rate-determining step can be determined using Tafel analysis following reported literature [50].
Electrochemical kinetic parameters of j_o, b, η and α were determined from Tafel Eqs. (4-6) [45], and cited in Table 1 for deposited Co, Fe, Mn, N and quaternary CFMN electrocatalysts from acetate bath. As shown in Fig. 4b, fabricated electrodes of quaternary CFMN electrocatalysts have smallest Tafel slope of 124 ± 4 mV/dec. Further, they have least negative value for overpotential and highest j_0 and α, which reveals their higher catalytic activity towards HER compared to the individual metal, and the reaction follows Volmer-Heyrovsky mechanism.

Table 1: Kinetic parameters of fabricated Ni, Co, Mn and Fe and their quaternary CFMN electrocatalysts from an acetate bath for HER in 1.0 M KOH at 298 K.

Catalysts	Co	Fe	Mn	Ni	Quaternary CFMN
η_{10} (mV)	–164	–264	–134	–194	–110
b (mV/dec)	144	179	147	146	124
j_o (A cm^{-2})	8.0*10^{-4}	3.68*10^{-4}	7.3*10^{-4}	7.8*10^{-4}	8.3*10^{-4}
α	0.20	0.08	0.20	0.22	0.23

Furthermore, Fig. 4c shows chronoamperometry of HER stability from quaternary CFMN electrocatalyst in 1.0 M KOH, at a constant potential of 0.10 V *vs.* RHE and 298 K. CFMN electrocatalyst shows excellent stability as current is retained at up to 86.3 % of its initial value after 4000 s of electrolysis. Fig. 4d shows LSV for HER, at a scan rate of 5.0 mV/s, after cycles 1 and 1000. It can be seen that HER's onset potential drops from −80 to −110 mV after 1000 cycles, which means quaternary CFMN electrocatalyst from acetate for HER is stable, but it has low durability, which needs to be improved. HER of CFMN electrocatalyst is compared with other materials from literature, and cited in Table 2.

Table 2: Comparison of HER activity and overpotential values from quaternary CFMN electrocatalysts with different catalysts reported in literature.

Catalyst	Medium	η_{10} (mV)	Reference
$NiCo_2S_4$ NW/NF arrays	1.0M KOH	-210	[53]
3D porous NF@G@Ni_3S_2 with a	1.0M KOH	119	[54]
CoNi-OOH-30(40)	1.0M KOH	-210	[55]
porous carbon spheres - doped Ni, Co - alloy	0.5M H_2SO_4	240	[56]
Fe (Ni/Co) hydroxy phosphate	1.0M KOH	145	[57]
quaternary CFMN electrocatalyst	1.0M KOH	-110	This work

Quaternary CFMN electrocatalyst had highest catalytic activity and least negative overpotential value of −110 ± 4 mV compared to other materials containing ternary or binary bifunctional catalysts.

Comparative electrocatalytic OER activity

Fig. 5a presents polarization curves (LSV) at 5 mV/s at 298 K for OER for deposited Co, Ni, Mn, Fe, and quaternary CFMN electrocatalysts in a 1.0 M KOH solution. As shown, OER onset potential required to produce a current density of 10 mA/cm^2 is decreased in following order: Fe (1.76 mV) > Mn (1.71 mV) > Ni (1.62 mV) > Co (1.59 mV). At a current density of 27 mA/cm^2 and overpotential of 1.68 V, LSV from quaternary CFMN precedes LSV from Fe, Mn, Ni and Co. This behavior indicates and confirms that quaternary CFMN alloy provides higher electrocatalytic properties than individual Fe, Mn, Ni and Co metals.

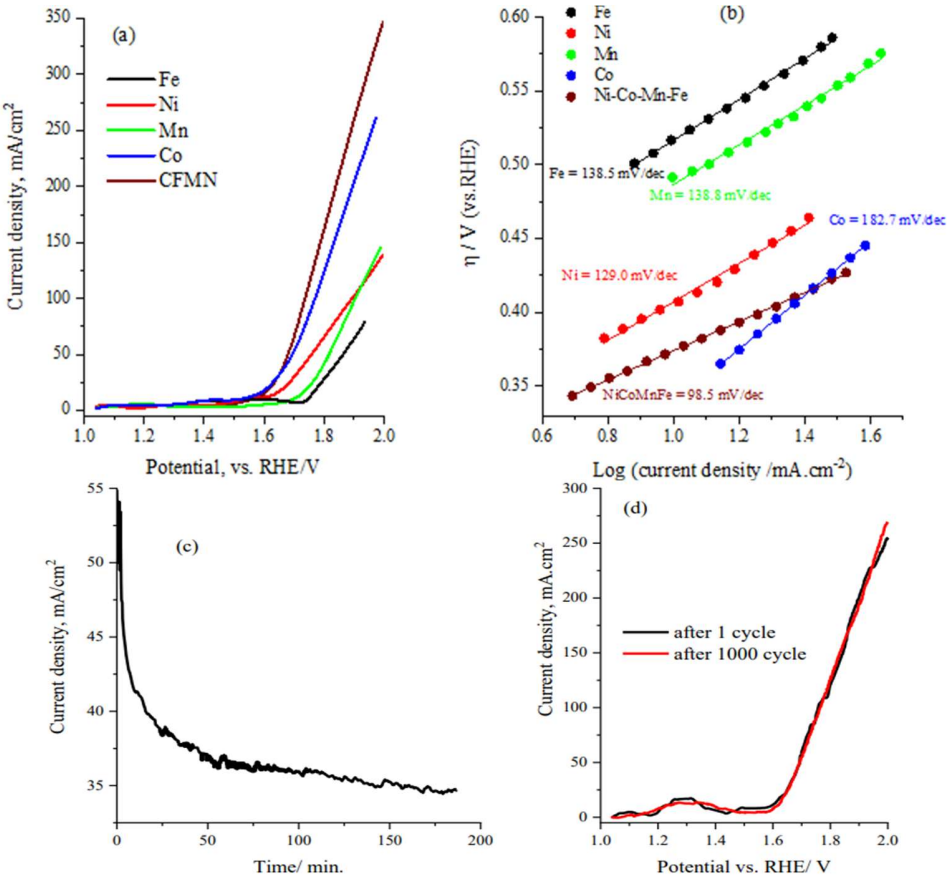

Figure 5: (a) LSV of 1.0 M KOH, at a scan rate of 5.0 mV/s, for OER, by Co, Fe, Mn, Ni, and their CFMN from acetate buffer with pH 4.6 at −1.15 V for 900 s; **(b)** Tafel plots of LSV for OER; **(c)** chronoamperometry current-time curve for deposited CFMN at 1.68 V *vs*. RHE for 12000 s; and **(d)** polarization curves for OER in 1.0 M KOH after 1 and 1000 cycles.

Quaternary CFMN electrode exhibits smallest onset potential of 1.54 mV *vs*. RHE, which suggests that it had higher catalytic activity towards OER among the studied electrodes in an alkaline solution. Fig. 5b shows corresponding Tafel plots of studied electrodes for OER. Quaternary CFMN electrode has the lowest Tafel slope value of 98.5 ± 4 mV/dec, which confirms superior activity of CFMN electrocatalyst compared to individual elements of Co, Fe, Mn and Ni.

Table 3 reports OER electrochemical kinetics parameters of overpotential (η_{10} = experimental values of potential at 10 mA/cm^2 –thermodynamics value of OER, which equals 1.23 V vs. RHE), Tafel slope, α coefficient, and exchange current density (*jo*) values of studied electrocatalysts. As has been shown in Table 3, fabricated quaternary CFMN electrode has lowest Tafel slope of 98.5 ± 4 mV/dec, and least positive values for onset potential and overpotential (η_{10}) values of 1.54 ± 0.002 V and 310 ± 4 mV, respectively. Additionally, it has highest j_o and α, which reveals its higher catalytic activity towards OER, and indicates that the reaction follows Volmer-Heyrovsky reaction. Also, quaternary CFMN has higher catalytic activity for OER than that when using the single metal.

Table 3: Kinetic parameters of fabricated Co, Fe, Mn, Ni, and their quaternary CFMN electrocatalysts from an acetate bath for OER in 1.0 M KOH at 298 K.

Catalysts	Co	Fe	Mn	Ni	Quaternary CFMN
Onset potential (mV) vs. RHE	1.59	1.76	1.71	1.62	1.54
η_{10} (mV)	360	530	480	390	310
b (mV/dec)	182.7	138.5	138.8	129	98.5
j_o (A/cm^2)	$9.5*10^{-3}$	$13.6*10^{-2}$	$13.6*10^{-2}$	$12.6*10^{-2}$	$45*10^{-2}$
α	0.17	0.21	0.21	0.23	0.29

Furthermore, durability and stability of quaternary CFMN electrocatalyst for OER were investigated in 1.0 M KOH via chronoamperometry, for 3 h, at a constant potential of 1.58 ± 0.002 V *vs*. RHE and after 1000 cycles. As shown in Fig. 6c, quaternary CFMN electrode exhibited good stability, with current being retained at 67.6% of its initial value. Moreover, Fig. 6d shows LSV of quaternary CFMN electrocatalyst durability for OER after 1 cycle and 1000 cycles, which reveals onset potential, and that current density remained constant after 1000 cycles. This confirms that fabricated CFMN electrocatalyst from acetate has excellent durability and stability for OER.

Table 4 reports OER activity and results of fabricated quaternary CFMN electrocatalyst as compared with state-of-the-art electrocatalysts reported in literature.

Table 4: Comparison of overpotential values for different catalysts for OER.

Catalyst	Medium	η_{10} (mV)	Ref.
Ni Fe Al O with metal vacancies	1.0 M NaOH	371	[58]
N-Ni_3S_2	1.0 M KOH	330	[59]
Fe Doped NiP	1.0 M KOH	270 @20 mA cm^{-2}	[60]
Fe Doped $Ni(OH)_2$/Ni Foam	1.0 M KOH	271 @20 mA cm^{-2}	[61]
Ni-Mn-Fe-Mo alloy	1.0 M KOH	570@1000 mA cm^{-2}	[62]
Ni-Fe-W-Mo alloy	1.0 M KOH	152	[63]
Co-Ni-Mn-Fe alloy	1.0 M KOH	310	This work

Conclusions

Development of electrocatalysts exhibiting robust catalytic activity in both HER and OER reactions is a critical requirement for advancing sustainable energy technologies. Non-precious bifunctional quaternary electrocatalysts from CFMN for water-splitting HER and OER have been usefully electrodeposited from acetate solutions. Physicochemical characterisation obtained from SEM, XRD and TEM analyses provides valuable insights into surface morphology, elemental composition and internal structure of quaternary CFMN electrocatalyst. Notably, electrodeposited quaternary CFMN electrocatalyst demonstrated highest catalytic activity, excellent stability, and a smaller Tafel slope for both HER and OER compared to single deposited Co, Fe, Mn and Ni electrodes. Findings can be useful in electrodeposition of multi-element electrocatalysts with desired morphologies and properties for efficient and long-lasting bifunctional electrocatalysts for energy conversion and storage applications.

Data availability

All data generated or analyzed during this study are included in this published article.

Competing interests

The authors declare no competing interests.

Abbreviations

Ag/AgCl: silver-silver chloride electrode
BCC: body-centred cubic
CFMN: cobalt-iron-manganese-nickel (Co-Fe-Mn-Ni)
CH_3COOH: acetic acid
$CH_3COONa.3H_2O$: sodium acetate trihydrate
$CoCl_2.6H_2O$: cobalt chloride hexahydrate
EDX: energy dispersive X-ray
FCC: face-centred cubic
$FeCl_3$: ferric chloride

H_2SO_4: sulphuric acid
HCP: hexagonal closed-packed
HER: Hydrogen evolution reaction
KOH: potassium hydroxide
LSV: linear sweep voltammetry
$MnCl_2.4H_2O$: manganese chloride
NaOH: sodium hydroxide
$NiCl_2.6H_2O$: nickel chloride hexahydrate
OER: Oxygen evolution reaction
RHE: reversible hydrogen electrode
SEM: scanning electron microscopy
TEM: transmission electron microscopy
XRD: x-ray diffraction

Symbols
α: transfer coefficient
j: current density
j_o: exchange current density
η: overpotential

Authors' contributions
Ibrahim El-Hallag: concept of present works; wrote the manuscript; elucidated electrochemical behavior; corresponding author. **Ahmad A. Al-Owais**: revised manuscript. **Safya El-Sharkawey**: did the experimental work.

References
1. Domanski DFR. The Electrodeposition of Metallic Molybdenum Thin-Film Coatings, from Aqueous Electrolytes Containing Molybdate Ions, M. Sc. thesis, Queen Mary, University of London. 2013:54-67.
2. El Rehim SA. Electroplating from acetate baths. Electrochim Acta. 1995;41:1413. https://doi.org/10.1016/0013-4686(95)00327-4
3. Wei Y, Wang R, Meng L et al. Hydrogen Generation from Alkaline $NaBH_4$ Solution Using a Dandelion-Like Co–Mo–B Catalyst Supported on Carbon Cloth. Int J Hydrog Ener. 2017;42:9945-9951. https://doi.org/10.1016/j.ijhydene.2016.12.130
4. Wang JG, Hua W, Li M et al. Structurally Engineered Hyperbranched NiCoP Arrays with Superior Electrocatalytic Activities Toward Highly Efficient Overall Water Splitting. A C S Appl Mater Interf. 2018;10:41237-41245. https://doi.org/10.1021/acsami.8b11576

5. Gao D, Liu R, Biskupek J et al. Modular Design of Noble-Metal-Free Mixed Metal Oxide Electrocatalysts for Complete Water Splitting. Ang Chem Int Ed Engl. 2019;58:4644-4648. https://doi.org/10.1002/anie.201900428
6. Chen L, Dong X, Wang Y et al. Separating Hydrogen and Oxygen Evolution in Alkaline Water Electrolysis Using Nickel Hydroxide. Nat Commun. 2016;7:11741. https://doi.org/10.1038/ncomms11741
7. Wu Y, He H. Direct-Current Electrodeposition of Ni–S–Fe Alloy for Hydrogen Evolution Reaction in Alkaline Solution. Int J Hydrog Ener.2018;43(4):1989-1997. https://doi.org/10.1016/j.ijhydene.2017.12.015
8. Patel PP, Hanumantha PJ, Datta MK et al. Cobalt Based Nanostructured Alloys: Versatile High Performance Robust Hydrogen Evolution Reaction Electro-catalysts for Electrolytic and Photo-electrochemical Water Splitting. Int J Hydrog Ener. 2017;42(27):17049-17062. https://doi.org/10.1016/j.ijhydene.2017.05.175
9. Najafpour MM, Renger G, Hołyńska M et al. Manganese Compounds as Water-Oxidizing Catalysts: From the Natural Water-Oxidizing Complex to Nanosized Manganese Oxide Structures. Chem Rev. 2016;116(5):2886-2936. https://doi.org/10.1021/acs.chemrev.5b00340
10. Turner JA. Sustainable Hydrogen Production. Science. 2004;305:972-974. https://doi.org/10.1126/science.1103197
11. Cao L, Luo Q, Liu W et al. Identification of Single-Atom Active Sites in Carbon-Based Cobalt Catalysts During Electrocatalytic Hydrogen Evolution. Nat Catal. 2019;2(2):134-141. https://doi.org/10.1038/s41929-018-0203-5
12. Yu F, Zhou H, Huang Y et al. High-Performance Bifunctional Porous Non-noble Metal Phosphide Catalyst for Overall Water Splitting. Nat Commun. 2018;9(1):2551. https://doi.org/10.1038/s41467-018-04746-z
13. Wei Y, Huang X, Wang J et al. Synthesis of Bifunctional Non-noble Monolithic Catalyst Co-W-P/carbon Cloth for Sodium Borohydride Hydrolysis and Reduction of 4-Nitrophenol. Int J Hydrog Ener. 2017;42(41):25860-25868. https://doi.org/10.1016/j.ijhydene.2017.08.148
14. Li Y, Huang B, Sun Y et al. Multimetal Borides Nanochains as Efficient Electrocatalysts for Overall Water Splitting. Small. 2019;15(1):e1804212. https://doi.org/10.1002/smll.201804212
15. Yu J, Cao Q, Li Y et al. Defect-Rich NiCeO x Electrocatalyst with Ultrahigh Stability and Low Overpotential for Water Oxidation. A C S Catal. 2019;9(2):1605-1611. https://doi.org/10.1021/acscatal.9b00191
16. Li S, Sirisomboonchai S, Yoshida A et al. Bifunctional CoNi/CoFe2O4 /Ni Foam Electrodes for Efficient Overall Water Splitting at a High Current Density. J Mater Chem A. 2018;6(39):19221-19230. https://doi.org/10.1039/C8TA08223E

17. Li C, Baek JB. Recent Advances in Noble Metal (Pt, Ru, and Ir)-Based Electrocatalysts for Efficient Hydrogen Evolution Reaction. A C S Omeg. 2020;5(1):31-40. https://doi.org/10.1021/acsomega.9b03550
18. Audichon T, Napporn TW, Canaff C et al. IrO2 Coated on RuO2 as Efficient and Stable Electroactive Nanocatalysts for Electrochemical Water Splitting. J Phys Chem C. 2016;120(5):2562-2573. https://doi.org/10.1021/acs.jpcc.5b11868
19. Cherevko S, Geiger S, Kasian O et al. Oxygen and Hydrogen Evolution Reactions on Ru, RuO2, Ir and IrO2 thin film electrodes in acidic and alkaline electrolytes: A comparative study on activity and stability. Cat Tod. 2016;262:170-180. https://doi.org/10.1016/j.cattod.2015.08.014
20. Mahmood J, Anjum MAR, Shin SH et al. Encapsulating Iridium Nanoparticles Inside a 3D Cage-Like Organic Network as an Efficient and Durable Catalyst for the Hydrogen Evolution Reaction. Adv Mater. 2018;30(52):e1805606. https://doi.org/10.1002/adma.201805606
21. Liu D, Dai L, Lin X et al. Chemical Approaches to Carbon-Based Metal-Free Catalysts. Adv Mater. 2019;31(13):e1804863. https://doi.org/10.1002/adma.201804863
22. Xiao Y, Zhang P, Zhang X et al. Bimetallic Thin Film NiCo-$NiCoO_2$@NC as a Superior Bifunctional Electrocatalyst for Overall Water Splitting in Alkaline Media. J Mater Chem A. 2017;5(30):15901-15912. https://doi.org/10.1039/C7TA03629A
23. Wei Y, Meng W, Wang Y et al. Fast Hydrogen Generation from $NaBH_4$ Hydrolysis Catalyzed by Nanostructured Co–Ni–B Catalysts. Int J Hydrog Ener. 2017;42(9):6072-6079. https://doi.org/10.1016/j.ijhydene.2016.11.134
24. Yu L, Zhou H, Sun J et al. Hierarchical Cu@CoFe Layered Double Hydroxide Core-Shell Nanoarchitectures as Bifunctional Electrocatalysts for Efficient Overall Water Splitting. Nano Ener. 2017;41:327-336. https://doi.org/10.1016/j.nanoen.2017.09.045
25. Zhu J, Yao Y, Chen Z et al. Controllable Synthesis of Ordered Mesoporous Mo2C@Graphitic Carbon Core-Shell Nanowire Arrays for Efficient Electrocatalytic Hydrogen Evolution. A C S Appl Mater Interf. 2018;10(22):18761-18770. https://doi.org/10.1021/acsami.8b04528
26. Ouyang T, Ye YQ, Wu CY et al. Heterostructures Composed of N-Doped Carbon Nanotubes Encapsulating Cobalt and β-Mo $_2$ C Nanoparticles as Bifunctional Electrodes for Water Splitting. Ang Chem Int Ed Engl. 2019;58(15):4923-4928. https://doi.org/10.1002/anie.201814262
27. Zhang F, Xi S, Lin G et al. Metallic Porous Iron Nitride and Tantalum Nitride Single Crystals with Enhanced Electrocatalysis Performance. Adv Mater. 2019;31:1806552. https://doi.org/10.1002/adma.201806552

28. Lai J, Huang B, Chao Y et al. Strongly Coupled Nickel-Cobalt Nitrides/Carbon Hybrid Nanocages with Pt-Like Activity for Hydrogen Evolution Catalysis. Adv Mater. 2019;31(2):e1805541. https://doi.org/10.1002/adma.201805541
29. Wei Y, Wang Y, Wei L et al. Highly Efficient and Reactivated Electrocatalyst of Ruthenium Electrodeposited on Nickel Foam for Hydrogen Evolution from $NaBH_4$ Alkaline Solution. Int J Hydrog Ener. 2018;43(2):592-600. https://doi.org/10.1016/j.ijhydene.2017.11.010
30. An L, Feng J, Zhang Y et al. Controllable Tuning of Fe-N Nanosheets by Co Substitution for Enhanced Oxygen Evolution Reaction. Nano Ener. 2019;57:644-652. https://doi.org/10.1016/j.nanoen.2018.12.094
31. Li F, Han GF, Noh HJ et al. Construction of Porous Mo3P/Mo Nanobelts as Catalysts for Efficient Water Splitting. Ang Chem Int Ed Engl. 2018;57(43):14139-14143. https://doi.org/10.1002/anie.201808844
32. Sun H, Xu X, Yan Z et al. Superhydrophilic Amorphous Co-B-P Nanosheet Electrocatalysts with Pt-Like Activity and Durability for the Hydrogen Evolution Reaction. J Mater Chem A. 2018;6(44):22062-22069. https://doi.org/10.1039/C8TA02999G
33. Liu X, Hu Q, Zhu B et al. Boosting Electro-chemical Hydrogen Evolution of Porous Metal Phosphides Nanosheets by Coating Defective TiO_2 Overlayers. Small. 2018;14(42):e1802755. https://doi.org/10.1002/smll.201802755
34. Wan Y, Zhang Z, Xu X et al. Engineering Active Edge Sites of Fractal-Shaped Single-Layer MoS_2 Catalysts for High-Efficiency Hydrogen Evolution. Nano Ener. 2018;51:786-792. https://doi.org/10.1016/j.nanoen.2018.02.027
35. Ibupoto ZH, Tahira A, Tang PY et al. MoS x @NiO Composite Nanostructures: An Advanced Nonprecious Catalyst for Hydrogen Evolution Reaction in Alkaline Media. Adv Funct Mater. 2019;29(7):1807562. https://doi.org/10.1002/adfm.201807562
36. Flis-Kabulska I, Sun Y, Zakroczymski T et al. Plasma Carburizing for Improvement of Ni-Fe Cathodes for Alkaline Water Electrolysis. Electrochim Acta. 2016;220:11-19. https://doi.org/10.1016/j.electacta.2016.10.084
37. Liu Y, Ying Y, Fei L et al. Valence Engineering via Selective Atomic Substitution on Tetrahedral Sites in Spinel Oxide for Highly Enhanced Oxygen Evolution Catalysis. J Amer Chem Soc. 2019;141(20):8136-8145. https://doi.org/10.1021/jacs.8b13701
38. Han L, Guo L, Dong C et al. Ternary Mesoporous Cobalt-Iron-Nickel Oxide Efficiently Catalyzing Oxygen/Hydrogen Evolution Reactions and Overall Water Splitting. Nano Res. 2019;12(9):2281-2287. https://doi.org/10.1007/s12274-019-2389-5

39. Kwong WL, Lee CC, Messinger J. Scalable Two-Step Synthesis of Nickel-Iron Phosphide Electrodes for Stable and Efficient Electrocatalytic Hydrogen Evolution. J Phys Chem C. 2017;121(1):284-292. https://doi.org/10.1021/acs.jpcc.6b09050
40. Qin F, Zhao Z, Alam MK et al. Trimetallic NiFeMo for Overall Electrochemical Water Splitting with a Low Cell Voltage. A C S Ener Lett. 2018;3(3):546-554. https://doi.org/10.1021/acsenergylett.7b01335
41. Li L, Cao X, Huo J et al. High valence metals engineering strategies of Fe/Co/Ni-based catalysts for boosted OER electrocatalysis. J Ener Chem. 2023;76:195-213. https://doi.org/10.1016/j.jechem.2022.09.022
42. Hao J, Wu K, Lyu C et al. Recent advances in interface engineering of Fe/Co/Ni-based heterostructure electrocatalysts for water splitting. Mater Horiz. 2023;10:2312-2342. https://doi.org/10.1039/D3MH00366C
43. Lu Z, Qian L, Tian Y et al. Ternary NiFeMn Layered Double Hydroxi-des as Highly-Efficient Oxygen Evolution Catalysts. Chem Commun (Camb). 2016;52(5):908-911. https://doi.org/10.1039/c5cc08845c
44. Anshul G, Mohammad F, Flamina A et al. Enhanced hydrogen storage in Mg catalysed by Cu–Ni–Co–Fe quaternary multi-component alloy. Int J Hydrog Ener. 2024;50:932-945. https://doi.org/10.1016/j.ijhydene.2023.08.243
45. Xin Li, Li B, Xinrong G et al. Enhanced the Overall Water Splitting Performance of Quaternary NiFeCrCo LDH: Via Increasing Entropy. Molecules. 2025;30:1461. https://doi.org/10.3390/molecules30071461
46. Wang Y, Liang Z, Zheng H et al. Recent Progress on Defect-Rich Transition Metal Oxides and Their Energy-Related Applications. Chem Asia J. 2020;15(22):3717-3736. https://doi.org/10.1002/asia.202000925
47. Wang J, Xu F, Jin H et al. Non-noble Metal-Based Carbon Composites in Hydrogen Evolution Reaction: Fundamentals to Applications. Adv Mater. 2017;29(14):1605838. https://doi.org/10.1002/adma.201605838
48. Zech N, Podlaha EJ, Landolt D. Anomalous Codeposition of Iron Group. Anomalous Code-position of Iron Group Metals: I. Experimental Results. J Electrochem Soc.1999;146(8):2886-2891. https://doi.org/10.1149/1.1392024
49. Dragos O, Lupu N, Grigorias M et al. Anomalous Codeposition of fcc NiFe Nanowires with 5-55% Fe and Their Morphology, Crystal Structure and Magnetic Properties. J Electrochem Soc. 2016;163:D83-D94. https://doi.org/10.1149/2.0771-603jes
50. Kieling VC. Parameters Influencing the Electrodeposition of Ni-Fe Alloys. Surf Coat Technol. 1997;96(2-3):135-139.https://doi.org/10.1016/S0257-8972(97)00078-9
51. Hatami E, Toghraei A, Darband GB. Electrodeposition of Ni–Fe Micro/Nano Urchin-Like Structure as an Efficient Electrocatalyst for Overall Water Splitting. Int J Hydrog Ener. 2021;46(14):9394-9405. https://doi.org/10.1016/j.ijhydene.2020.12.110

52. Krstajić N, Popović M, Grgur B et al. On the Kinetics of the Hydrogen Evolution Reaction on Nickel in Alkaline Solution - Part I. J Electroanalyt Chem. 2001;512(1-2):16-26. https://doi.org/10.1016/S0022-0728(01)00590-3
53. Sivanantham A, Ganesan P, Shanmugam S. Hierarchical $NiCo_2S_4$ Nanowire Arrays Supported on Ni Foam: An Efficient and Durable Bifunctional Electrocatalyst for Oxygen and Hydrogen Evolution Reactions. Adv Funct Mater. 2016;26(26):4661-4672. https://doi.org/10.1002/adfm.2016 00566
54. Jin C, Zhou N, Wang Y et al. 3D Porous and Self-Supporting Ni foam@graphene@Ni3S2 as a Bifunctional Electrocatalyst for Overall Water Splitting in Alkaline Solution. J Electroanalyt Chem. 2020;858;113795. https://doi.org/10.1016/j.jelechem.2019.113795
55. Yu C, Lu J, Luo L et al. Bifunctional Catalysts for Overall Water Splitting: Coni Oxyhydroxide Nanosheets Electrodeposited on Titanium Sheets. Electrochim Acta. 2019;301:449-457. https://doi.org/10.1016/j.electacta.2019.01.149
56. Xu Y, Dong X, Miao J et al. Facile Preparation of Ni, Co - Alloys Supported on Porous Carbon Spheres for Supercapacitors and Hydrogen Evolution Reaction Application. Int J Hydrog Ener. 2020;45(3):1466-1476. https://doi.org/10.1016/j.ijhydene.2019.11.074
57. Babar PT, Lokhande AC, Jo E et al. Facile Electrosynthesis of Fe (Ni/Co) Hydroxyphosphate as a Bifunctional Electrocatalyst for Efficient Water Splitting. J Ind Eng Chem. 2019;70:116-123. https://doi.org/10.1016/j.jiec.2018.09.041
58. Jin D, Yu, Lee Y et al. NixRh1-xOy Composite Nanofibres as Highly Efficient and Robust Oxygen Evolution Electrocatalysts. J All Comp. 2020;836:155309. https://doi.org/10.1016/j.jallcom.2020.155309
59. Li J, Song J, Huang BY et al. Enhancing the Oxygen Evolution Reaction Performance of NiFeOOH Electrocatalyst for Zn-Air Battery by N-Doping. J Catal. 2020;389:375-381. https://doi.org/10.1016/j.jcat.2020.06.022
60. Wang P, Pu Z, Yi L et al. Nickel, Iron-Doped Nickel Phosphide Nanosheet Arrays: An Efficient Bifunctional Electrocatalyst for Water Splitting. A C S Appl Mater Interf. 2017;9(31):26001-26007. https://doi.org/10.1021/acsami.7b06305
61. Ren JT, Yuan GG, Weng CC et al. Uniquely Integrated Fe-Doped Ni(OH)2 Nanosheets for Highly Efficient Oxygen and Hydrogen Evolution Reactions. Nanoscale. 2018;10(22):10620-10628. https://doi.org/10.1039/c8nr01655k
62. Liu H, Xi C, Xin J et al. Free-standing Nanoporous NiMnFeMo Alloy: An Efficient Non-precious Metal Electrocatalyst for Water Splitting. Chem Eng J. 2021;404:126530. https://doi.org/10.1016/j.cej.2020.126530
63. Zhang P, Tan W, He H et al. Binder-Free Quaternary Ni–Fe–W–Mo Alloy as a Highly Efficient Electrocatalyst for Oxygen Evolution Reaction. J All Comp. 2021;853:157265. https://doi.org/10.1016/j.jallcom.2020.157265